Advanced Ceramics Progress: Vol. 8, No. 2, (Spring 2022) 12-26

Materials and Energy Research Center
MERC

Contents lists available at ACERP

Advanced Ceramics Progress

Journal Homepage: www.acerp.ir

Original Research Article

Characterization and Performance Evaluation of Fabricated TFN-RO Membranes in the Presence of MFI Type Zeolite

Safoura Bakhodaye Dehghanpour [a], Fahime Parvizian [b,*], Vahid Vatanpour [c,*]

[a] *PhD Candidate, Department of Chemical Engineering, Faculty of Engineering, Arak University, Arak, Markazi, Iran*
[b] *Associate Professor, Department of Chemical Engineering, Faculty of Engineering, Arak University, Arak, Markazi, Iran*
[c] *Associate Professor, Department of Applied Chemistry, Faculty of Chemistry, Kharazmi University, Tehran, Tehran, Iran*

* Corresponding Authors' Emails: f-parvizian@araku.ac.ir (F. Parvizian); vahidvatanpour@khu.ac.ir (V. Vatanpour)
URL: https://www.acerp.ir/article_154054.html

ARTICLE INFO

Article History:

Received 07 May 2022
Received in revised form 08 August 2022
Accepted 16 August 2022

Keywords:

Reverse Osmosis
Desalination
Interfacial Polymerization
Antifouling

ABSTRACT

Thin Film Composite (TFC) membranes were fabricated by Interfacial Polymerization (IP) of M-Phenylene Diamine (MPD) and Tri-Mesoyl Chloride (TMC) on Polysulfone (PSf) support in the presence of hydrothermally synthesized TS-1 zeolite as an additive blended in the MPD aqueous solution. Formation of the MFI structure (Pentasil Zeolite), presence of extra-framework TiO_2, and zeolite particle size were investigated through X-Ray Diffraction (XRD), Fourier Transform Infrared Spectroscopy (FTIR), and Field Emission Scanning Electron Microscopy (FE-SEM) analyses, respectively. In addition, the effect of the TS-1 zeolite concentration in the range of 0-0.02 wt. % on the desalination and antifouling performance of the reverse osmosis membranes was evaluated in this study. The obtained results revealed that the membrane containing zeolite at the optimal concentration of 0.005 wt. % had the smoothest surface (RMS: 21.05 nm) and lowest contact angle (51.32°), thus exhibiting the best performance in the water flux of 47.5 $Lm^{-2}h^{-1}$ at 15 bars. In addition, compared to the unfilled TFC membrane, the rejection percentage of NaCl was calculated as 96.7 % (2000 ppm). Further, the antifouling ability of the membranes in the face of Bovine Serum Albumin (BSA) showed the excellent fouling resistance of the zeolite-modified membranes.

https://doi.org/10.30501/acp.2022.348785.1094

1. INTRODUCTION

The population growth, climate change, and excessive use of water resources are among the factors threatening the existing water supplies and causing serious problems many communities are facing that significantly increase the demands for new desalination technologies and water resources [1]. Therefore, the seawater desalination and wastewater reuse is an appropriate approach to solving the problem of water scarcity [2]. Desalination technology is classified into thermal and membrane-based processes based on their separation mechanism [3,4]. Membrane separation technology is the most suitable option for separating a wide range of contaminants from water due to its relatively low energy consumption, simple operating process, low required space, and no requirement of chemical additives [5,6]. Due to the simplicity and relatively low cost of the

Please cite this article as: Bakhodaye Dehghanpour, S., Parvizian, F., Vatanpour, V., "Characterization and Performance Evaluation of Fabricated TFN-RO Membranes in the Presence of MFI Type Zeolite", ***Advanced Ceramics Progress***, Vol. 8, No. 2, (2022), 12-26. https://doi.org/10.30501/acp.2022.348785.1094

available types of energy compared to the thermal processes, most water desalination units in the world currently employ Reverse Osmosis (RO) technology [7]. Cellulose acetate and its derivatives as well as Polyamide (PA) are widely used in manufacturing polymeric RO membranes. These membranes are asymmetric that are made of two categories of integrally-skinned asymmetric membranes and Thin Film Composites (TFC) [8,9]. PA-TFC membranes have a major share of the RO membrane market due to their high salt rejection and water flux potency, modification of the TFC membrane layers separately, relatively low overall manufacturing cost, and high mechanical strength [2]. One of the main challenges in application of RO membranes is fouling with contaminants inside the membrane pores or on its surface, which leads to a decrease in the proper performance of the membrane by affecting the water flux, permeation quality, and salt rejection. Therefore, pre-treatment of feed water [10] and modification of the membrane active thin layer with different compounds can be a suitable solution to improvement of the membrane performance and fouling reduction [11]. To this end, many researchers developed different methods such as considering a change in the membrane monomers [12], addition of organic materials [13], surface modification methods (physical and chemical) [14-16], and nanotechnology [17]. Among these procedures, several studies have been conducted to fabricate Thin Film Nanocomposite (TFN) membranes using nanotechnology and introduction of nanomaterials based on some advantageous groups such as hydroxyl and carboxyl into the membrane [18-22]. Several compounds namely Titanium Dioxide (TiO_2) [23-25], Graphene Oxide (GO) [26], Carbon Nano-Tubes (CNTs) [27], Metal-Organic Frameworks (MOFs) [28,29], and zeolites [30,31] are used to enhance water diffusion and salt rejection as well as fouling reduction.

Zeolites are nanomaterials with excellent capability to enhance the membrane performance owing to their chemical stability and good retardation. They are crystalline aluminosilicate materials with uniform pore sizes in which rejection mechanisms are defined based on the ion exchange and molecular screening. In other words, ions with low hydration radii show greater diffusion through the structure of zeolite cavities. In addition, Nano-zeolites facilitate adsorption of cations by presenting negatively charged centers on the membrane surface that can improve the separation performance [17,32]. Jung et al. [33] reported the fabrication of TFC-RO membranes by dispersing NaA zeolite nanoparticles in the PA films. The modified membranes showed better permeability than the unfilled ones. The idea of using zeolite was suggested due to the structure of pores and consequently, hydrophilicity with antibacterial properties led to introduction of membranes with high performance where the flux was twice as high as that of the unmodified membrane in the membrane with the concentration of 0.4 w/v % zeolite. Fathizadeh et al. [34] added NaX nano-zeolite to the PA layer. The fabricated membranes then improved the surface properties, thus ensuring more water permeability than the zeolite-free membrane. The obtained results showed a decrease and increase in the thickness and pore size of the active thin film, respectively. Dong et al. [35] utilized synthesized NaY zeolite nanoparticles to prepare TFN membranes. Zeolite nanoparticles under an optimal loading of 0.15 wt. % zeolite in a diamine solution increased the flux from 39.6 $Lm^{-2}h^{-1}$ in a membrane without zeolite up to 74.17 $Lm^{-2}h^{-1}$ by forming nano-spaces in the interfacial and possessing a porous structure. Of note, the rejection with 2000 ppm feed salt concentration remained constant at about 98.8 %. Cay-Durgun et al. [36] in their experiments increased the water permeation up to 1.4 times of that of the TFC membrane by embedding 0.30 wt. % of Linde type A zeolite to the RO membrane. In addition, the solute rejection in their study increased from 97.4 up to 97.9 %. Membranes fabricated by this zeolite showed better stability than the TFC membrane in long-term desalination. Incorporation of S-Beta zeolite with hydrophilic nature into the PA layer increased the water flux and NaCl rejection from 25.36 to 65.25 $Lm^{-2}h^{-1}$ and from 97 to 97.33 %, respectively at an optimal content of 0.05 wt. % [37].

MFI type zeolites are also used to fabricate membranes containing zeolite nanoparticles [38]. For example, PA composite membranes were synthesized through Interfacial Polymerization (IP) method based on commercial Polysulfone (PSf) substrate in the presence of silicalite to evaluate the desalination performance. The surface roughness of the fabricated membrane was similar to that of the commercial zeolite-free membrane. Increasing the zeolite loading up to 0.5 wt. % increased water flux up to 9.86 $Lm^{-2}h^{-1}$, which was higher than that of the unmodified membrane, but NaCl rejection (98.1) decreased by 50 % as the density of the PA layer decreased [39]. Huang et al. [40] in a study investigated the effect of silicalite-1 with a pore size of 0.56 nm in the TFC membrane and proved that the surface of S-PA membrane was more hydrophilic than that of the bare membrane, hence excellent water permeability and large-scale seawater desalination.

Titanium Silicate-1 (TS-1) is another member of the MFI type that is acknowledged to be a milestone in oxidation reactions as an excellent catalyst [41]. Synthesized by isomorphous substitution of silicon with titanium, this zeolite, similar to Silicalite-1, is characterized by three-dimensional pores and channels with dimensions of 0.56 nm × 0.53 nm. This zeolite is also characterized by a different morphology of regular cubic to irregular blackberry-like [42-44]. So far, this zeolite has been used as an additive in gas separation and pervaporation membranes [45,46]. However, in some limited cases, this zeolite is generally utilized as a zeolite membrane with desalination applications. For example,

Zhang et al. [47] employed the periodic secondary growth method to fabricate the TS-1 bilayer membrane on a seeded support. Such a membrane enjoys a hydrophobic and flawless structure. However, to the best of the authors' knowledge, there is no report on the fabrication of the TFN-RO membrane based on the incorporation of this zeolite as a nanoparticle using the IP method. In this regard, the current study utilized a hydrophilic TS-1 zeolite nanoparticle as an additive to the aqueous phase to fabricate TFN-RO membrane through the IP method. The main objective here was to enhance the membrane performance by taking advantage of the interesting properties of TS-1 such as negative charged groups and molecular sieving properties, to name a few. In order to determine how zeolite concentration affects the membrane performance, a series of TFN membranes were fabricated under different zeolite loadings. In addition, the membranes were characterized followed by their preparation. The characteristics of the RO membranes such as the structure of their surface morphology and hydrophilicity under different zeolite nanoparticle loadings were investigated. Water permeability and separation performance were also evaluated based on the separation tests. Further, the antifouling potential of all membranes in the face of the BSA protein as a foulant was studied. It was expected that followed by the insertion of the TS-1 zeolite into the active thin layer of the TFN-RO membranes, the performance and fouling resistance would significantly improve.

2. EXPERIMENTAL

2.1. Materials

All materials needed for the synthesis of the MFI zeolite namely Tetra-n-butyl orthotitanate (TBOT, 97 wt. %), tetrapropylammonium hydroxide solution (TPAOH, 40 wt. %), tetraethyl orthosilicate (TEOS, 98 wt. %), and isopropanol were purchased from Merck company. In order to fabricate the membrane support, Dimethylformamide (DMF, Merck, Germany) and polysulfone (PSf, MW: 58,000 $gmol^{-1}$, BASF, Germany), and a non-woven polyester fabric were used. In addition, M-Phenylenediamine (MPD, Sigma-Aldrich, USA), triethylamine (TEA, Merck, Germany) and (+) 10-camphor sulfonic acid (CSA, Merck, Germany), trimesoyl chloride (TMC, Merck, Germany), and n-hexane dehydrated by molecular sieve (Merck, Germany) were utilized to obtain the barrier layer. Of note, Bovine serum albumin (BSA, MW: 67,000 $gmol^{-1}$) and NaCl were purchased from Merck company.

2.2. Synthesis of MFI Zeolite

The hydrothermal synthesis of TS-1 zeolite was accomplished according to the protocol proposed by Du et al. [48]. To this end, 7.5 g TEOS was added dropwise into 9.3 g TPAOH (25 % aqueous solution) as a template and 2.3 g distilled water with stirring. After that, 0.32 g TBOT was dissolved in 1.2 g isopropanol and added slowly into the above mixture. The prepared solution was kept stirring for 20 min at 25 °C. To hydrolyze and remove the alcohol, the temperature of the solution was raised up to 70 °C under vigorous stirring for 2 h. Then, 15 g distilled water was added to the precursor mixture and stirring continued for another 20 min. An autoclave with Teflon-lined steel was used to heat the solution for 72 h at 160 °C. To obtain the synthesized zeolite, the resultant product was washed by centrifugation with ethanol and distilled water. Calcination was then performed by calcining the solid at 550 ° C for 6 h after it had been dried overnight at 60 °C.

2.3. Fabrication of TS-1/RO Membrane

The fabrication process of TFC-RO membranes involves two steps: preparing the porous PSf support and generating the PA layer on the support. The phase inversion method was employed to prepare the PSf support. The formulation of the casting solution is as follows: PSf (19 wt. %) should be added into the DMF (81 wt. %) as a solvent and kept stirring until a homogeneous solution is obtained and then, it should be heated for four hours at 50 ° C to eliminate air bubbles. Casting of PSf solution was then conducted using a film applicator on polyester fabric. The cast films were immediately transferred to a bath containing distilled water as the non-solvent and preserved for two hours. The TFC-RO membrane including a PA layer on the support was prepared through interfacial polymerization according to the method proposed by Safarpour et al. [24]. The prepared support was then dipped in a solution containing MPD (2.0 wt. %), TEA (2.0 wt. %), and CSA (2.0 wt. %) for 10 min and then removed. The remained solution was drained of the surface by a glass roller. Subsequently, the MPD-impregnated membrane was fixed on a glass plate, and an organic solution of TMC (0.1 wt. %) in n-hexane was spread on its top surface and allowed to subject for one min. The membrane was washed using n-hexane to remove the unreacted monomers from the surface and then cured for 10 min at 70 °C. To fabricate the TFN membranes containing zeolite, first, the same amount of zeolite was added to the distilled water and n-hexane separately and then, ultrasonication was used for 30 min to evaluate the stability of zeolite dispersion in aqueous and organic phases. The zeolite in the n-hexane was immediately precipitated after ultrasonication while it remained well dispersed in water for hours due to the hydrophilic essence of synthesized zeolite. Accordingly, the membranes containing zeolite were prepared by dispersing different loadings of zeolite (0.002, 0.005, 0.01, and 0.02 wt. % based on the weight of the aqueous solution) in distilled water and then, the zeolite solution was added to the aqueous solution for an IP process. The

rest of the procedure is the same as what was already described. The prepared membranes were called TFC for non-zeolite membrane and TFN-Z-X where X indicates the concentration of zeolite in the aqueous phase.

2.4. Characterization

X-Ray Diffraction (XRD) analysis of TS-1 zeolite was performed using Philips X-ray diffractometer model with the current and voltage of 25 mA and 30 kV, respectively, and CuKα radiation (λ = 0.154 nm). Phase analysis was then performed using X'Pert HighScore Plus version 2.0 software. Further, Attenuated Total Reflection-Fourier Transform Infrared (ATR-FTIR) was taken into consideration to study the membrane surface modification in the range of 650-4000 cm^{-1} by SPECAC Golden Gate (England). Fourier Transform Infrared Spectra (FTIR) was also recorded on Perkin Elmer Spectrum RX1 using KBr pellet method from 400 to 4000 cm^{-1}. Furthermore, Field Emission Scanning Electron Microscopy (FE-SEM) model TESCAN was employed to study the microstructure of the synthesized zeolite as well as the surface and cross-sectional properties of the fabricated membranes. For cross-sectional analysis, all membranes were broken down in liquid nitrogen to prevent deformation. In addition, Energy Dispersive X-ray (EDX) was employed to verify the existence of Ti on zeolite and dispersion of zeolite in the membrane structure. Determination of topology and parameters of the surface roughness of membranes with a 5 µm× 5 µm scan area was recorded through Atomic Force Microscopy (AFM) analysis Park scientific instruments-C_p auto probe model. Moreover, a contact angle analyzer was utilized to assess the hydrophilicity of membrane surfaces. In order to decrease the experimental errors and increase accuracy, the measurements were made at five different membrane points, and the mean contact angle value was calculated.

2.5. Membrane Performance Evaluation

Several experiments were done to evaluate the RO performance considering the pure water flux, NaCl rejection, and antifouling by permeating aqueous solution through the membrane films with the area of 36 cm^2 in a cross-flow filtration system. In order to obtain a steady flux, the membranes were pre-compacted at 20 bars. The experiments were done at the ambient temperature and pressure of 15 bars. The amount of pure water flux is measured through Equation (1).

$$J = \frac{V}{A \times t} \quad (1)$$

where V, A, t, and J are the volume of permeate flux (L), effective area of membrane (m^2), test time (h), and permeate flux ($Lm^{-2}h^{-1}$), respectively.

Moreover, NaCl rejection was determined using 2000 ppm NaCl solution. In addition, the amount of (R(%)) can be calculated through Equation (2).

$$R(\%) = \left(1 - \frac{C_P}{C_f}\right) \times 100 \quad (2)$$

where C_p and C_f indicate the salt concentration in the permeate and feed solution, respectively, both determined by a conductometer.

Followed by adding BSA protein (200 ppm) to the NaCl solution (2000 ppm), the anti-fouling ability of the membranes for 90 min was studied. Also, the permeated water volume was quantified to determine the flux.

To minimize the experimental errors, all experiments were conducted at least three times for each membrane, and their mean values were claculated.

3. RESULTS AND DISCUSSION

3.1. TS-1 Zeolite Characterization

Figure 1a demostrates the XRD pattern of TS-1 zeolite in the range of 2θ=5-60°. As observed, the synthesized zeolite shows the characteristic diffraction peaks of the MFI topology at 2θ=7.9°, 8.8°, 23.0°, 23.9°, and 24.4° [49] that correspond to the d-spacing 11.2, 10.08, 3.86, 3.73, and 3.66 Å, respectively. The diffraction peak of 2θ=25.4° shows the presence of anatase TiO_2. This peak in the XRD pattern of the synthesized zeolite is undetectable mainly due to the high dispersion of TiO_2 formed during zeolite crystallization [48].

Figure 1b illustrates the FTIR spectroscopy of the synthesized zeolite. The appearance of vibration adsorption bands at 552, 807, 960, 1100, and 1230 cm^{-1} agrees with the typical FTIR spectrum of the TS-1 zeolite [50]. The band at 552 cm^{-1}, which is attributed to the vibrations of double five-membered rings, belongs to the characteristic band of MFI topology, and the band at 1230 cm^{-1} corresponds to the TiO_4 and SiO_4 tetrahedral asymmetric stretching in the zeolite structure [49,51]. The band at 552 cm^{-1} and weak band at 628 cm^{-1} are indictive of the presence of TiO_2 [52,53]. The adsorption band at 960 cm^{-1} attributed to the stretching vibration of SiO_4 units adjacent to the structural titanium is indicative of the insertion of Ti into the zeolite framework. Of note, IR absorptions at 451, 807, and 1100 cm^{-1} are said to the internal vibrations of TiO_4 and SiO_4 and the broad band at 3430 cm^{-1} shows the presence of hydroxyl groups [54,55].

Figure 1c presents the FE-SEM image of the morphology and particle diameter of the synthesized zeolite. The average size of the synthesized zeolite particles is about 180 nm, indicating an aggregated structure with a blackberry-like shape [56]. The EDX mapping analysis was then done to ensure the presence of Ti on the zeolite surface, the results of which are given

in Figure 1d. The results confirmed the presence of Ti on the surface of the synthesized zeolite with a relatively uniform distribution (Red dots indicate the presence of Ti). The EDX survey (Figure 1e) was also done to confirm the presence of Ti. One of the notable properties of TS-1 zeolite is the amount of tetrahedral Ti inserted into the zeolite framework, which is substituted by Si atoms. At the same time, this substitution is bound to a restriction. To be specific, given that Ti has a larger atomic radius than that of the stable silicalite-1 structure, it causes changes in the unit cell parameters during insertion.

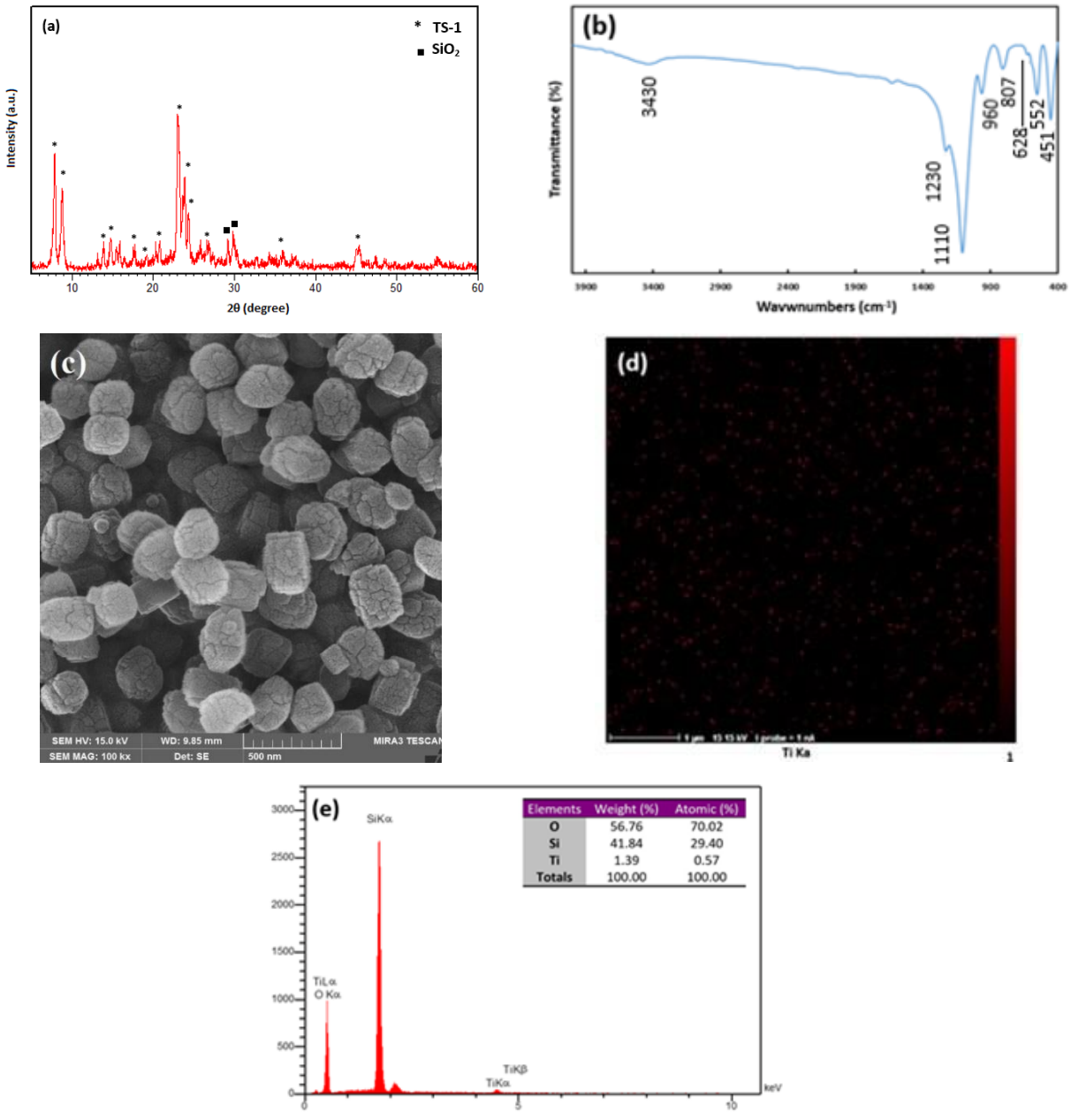

Figure. 1. (a) XRD pattern, (b) FTIR spectrum, (c) FE-SEM image, (d) EDX map of Ti element, and (e) EDX spectrum of the synthesized TS-1 zeolite

According to the results, the highest amount of Ti that can enter the lattice is about 2.5 A while the rest of Ti in the synthesis solution will not be able to enter the scaffold, hence converted to extraframework TiO_2 phases [57]. It should be noted that the presence of extraframework Ti can be confirmed through the FTIR analysis.

3.2. Structure and Properties of the Membranes

FE-SEM analysis was done to assess the surface and cross-sectional morphology of the membranes prior to and followed by the zeolite introduction. Figure 2 shows the effect of different zeolite loadings on the cross-sectional morphology of the fabricated membranes. For all asymmetric membranes, the formation of a PA layer on the spongy structure of the PSf support is observable. According to the images, the thickness and support values of the PA layer were calculated as 250-350 nm and 30-40 µm, respectively. Of note, the thickness of the PA layer did not change significantly with the introduction of zeolite probably due to the small amount of the used zeolite.

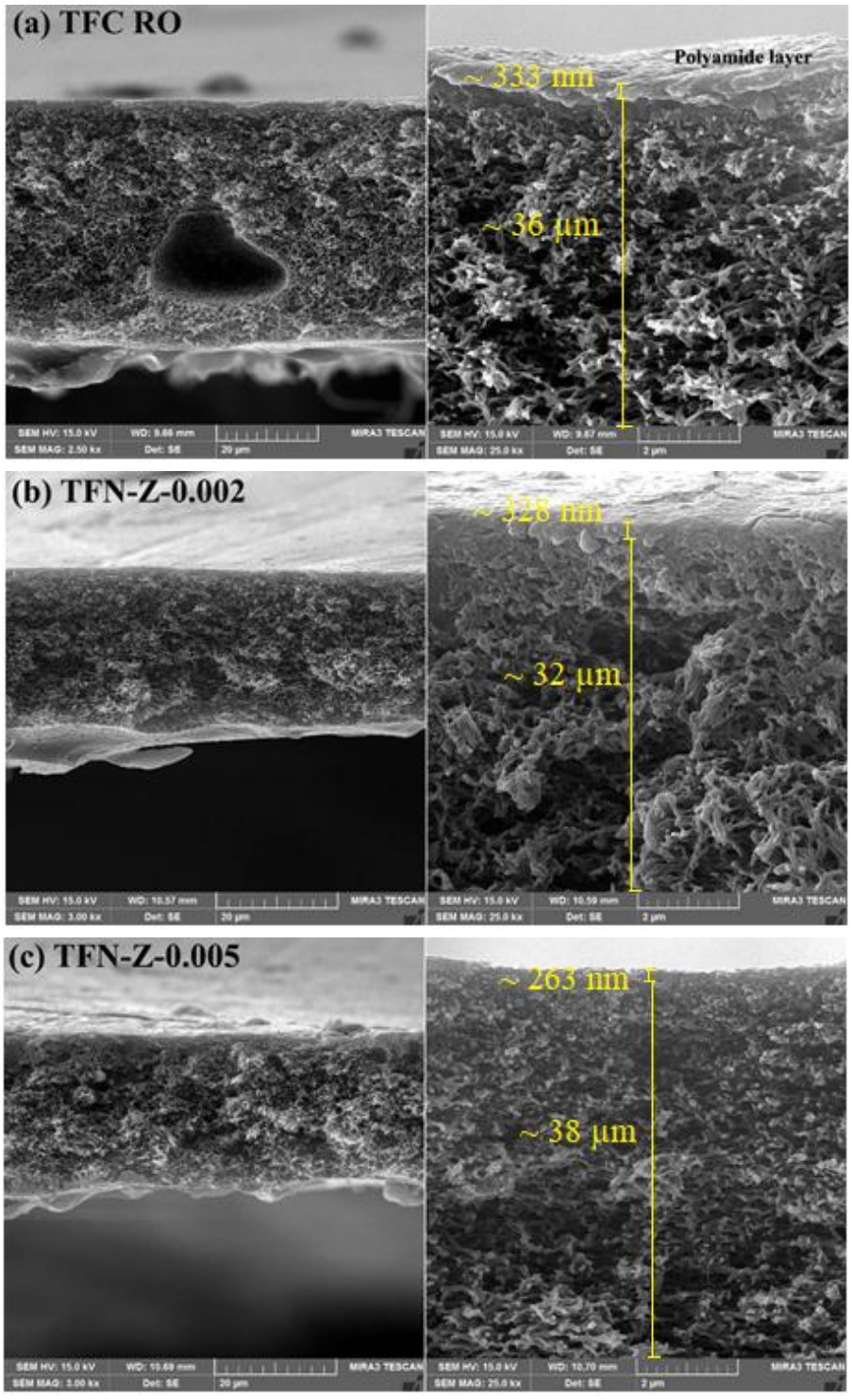

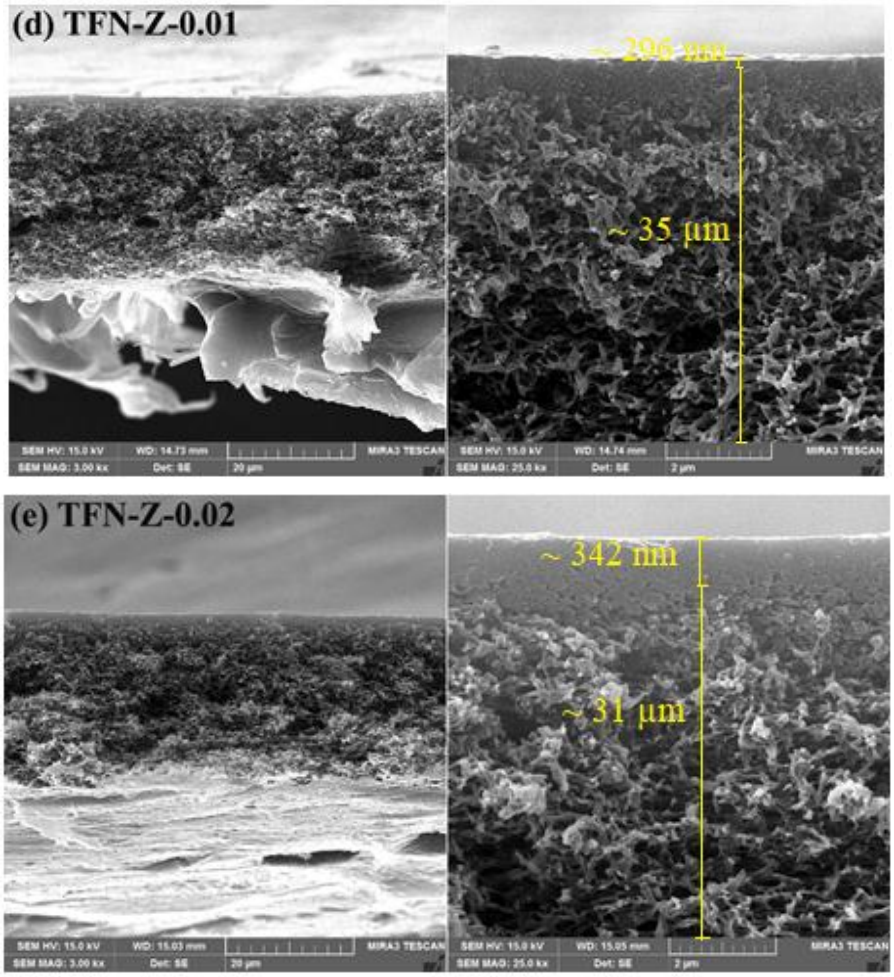

Figure 2. The cross-sectional FE-SEM images of (a) TFC, (b) TFN-Z-0.002, (c) TFN-Z-0.005, (d) TFN-Z-0.01, and (e) TFN-Z-0.02 membranes

Figure 3 shows the upper surface of all membranes. Clearly, all membranes have a hill and valley morphology, which is a common structure among the PA membranes formed through the polymerization of the interface between MPD and TMC [35]. However, it seems that upon adding zeolite to the PA layer, the surface morphology of the membranes will considerably chanege. Upon inserting 0.002 and 0.005 wt. % zeolite into the polymerization solution, the surfaces of the membranes will gradually get smoother than the TFC membrane.

Changes in the miscibility and kinetics of the aqueous and organic solution induced by zeolite as well as the interaction between TS-1 and MPD are the key factors that alter the membrane morphology and reduce the surface roughness [30], as observed in the TFN-Z-0.002 and TFN-Z-0.005 membranes (Figures 3b and 3c, respectively). On the contrary, followed by increasing the zeolite concentration, the surface morphologies of the TFN-Z-0.01 and TFN-Z-0.02 membranes will get rougher probably due to the formation of larger zeolite particles containing smaller particles. Similar trends have been detected by other researchers [58,59]. In order to further investigate the morphology and surface roughness of the fabricated membranes, AFM analysis is discussed in detail in the following.

Given that zeolite particles were indistinguishable on the surface and cross-section of the TFN membranes, the EDX survey was employed to confirm the presence of zeolite (Ti and Si elements) on the TFN-Z-0.005 membrane surface. As illustrated in Figure 4a, the EDX map analysis shows a relatively uniform distribution of zeolite on the membrane surface. In this analysis, green and red dots indicate the attendance of Si and Ti elements on the surface of the zeolite-modified membrane, respectively.

In addition, the EDX spectrum of the modified membrane given in Figure 4b confirms the presence of Ti and Si on the surface of TFN-Z-0.005 membrane, thus confirming the presence of zeolite in TFN membranes.

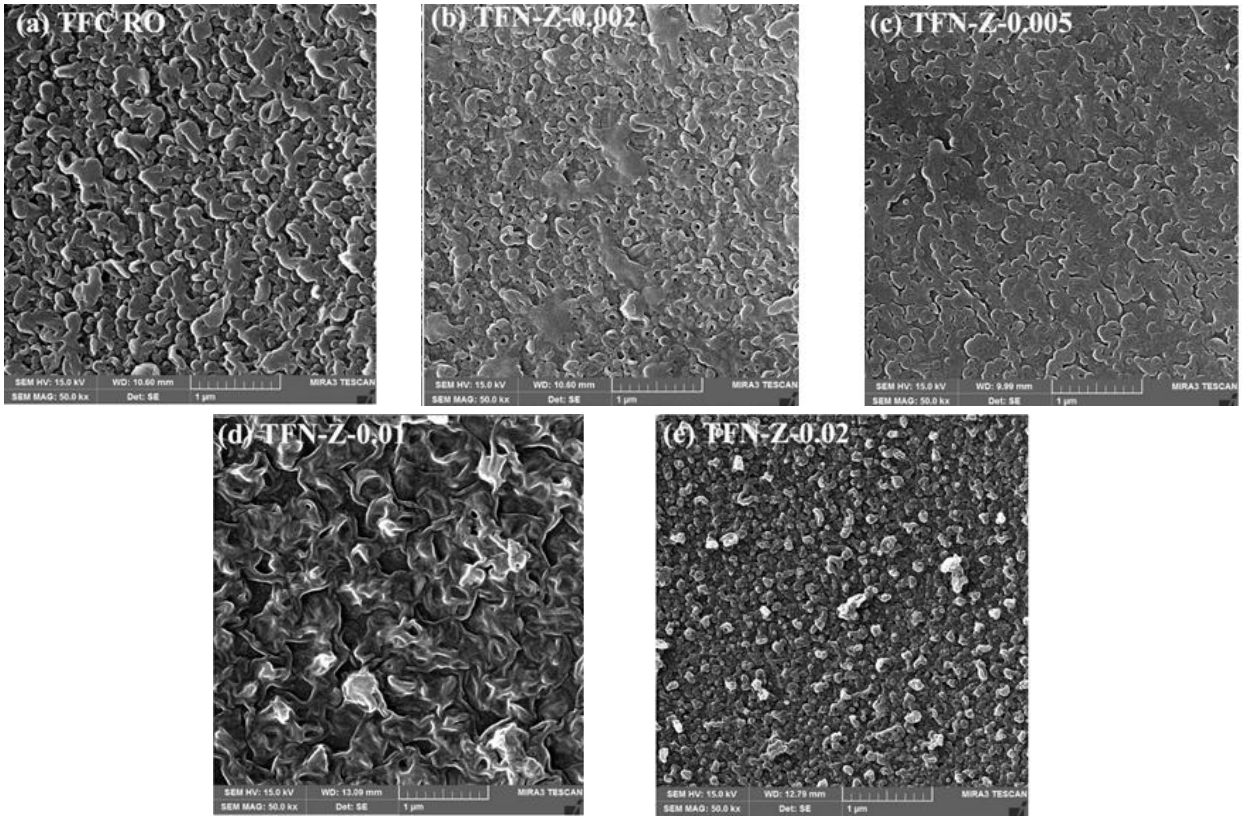

Figure 3. Surface FE-SEM images of (a) TFC, (b) TFN-Z-0.002, (c) TFN-Z-0.005, (d) TFN-Z-0.01, and (e) TFN-Z-0.02 membranes

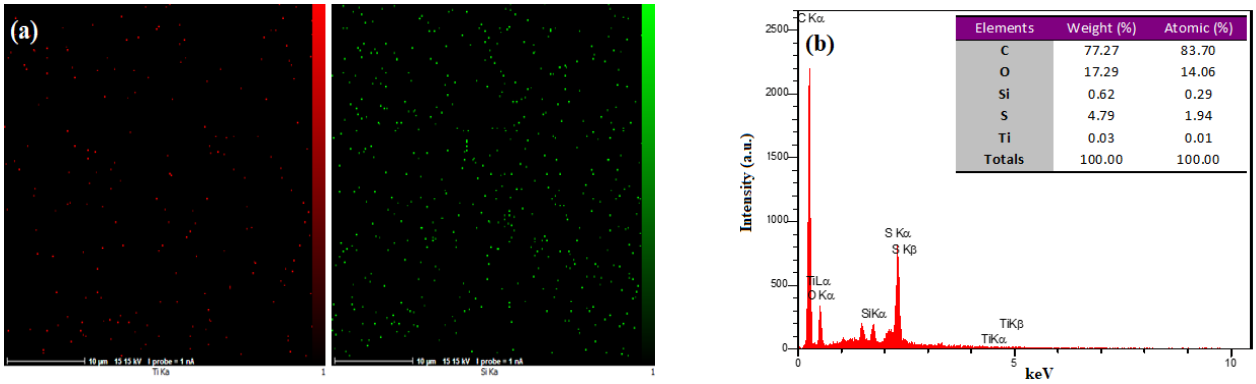

Figure 4. (a) EDX map of Ti and Si element and (b) EDX spectrum of TFN-Z-0.005 membrane

Figure 5 presents the results from the AFM analysis that help examine the surface properties with the scan size of 5 µm × 5 µm. Table 1 lists the average arithmetic (S_a) and Root Mean Square (RMS) roughness as the parameters that determine the surface roughness. The trend observed in this analysis is similar to that in the FE-SEM results according to which, the lowest surface roughness is attributed to the TFN-Z-0.005 membrane with the smoothest surface. As mentioned earlier, the presence of zeolite can change the reaction rate between the organic and aqueous monomers. On the contrary, the chemical bonding between the TiO_2 and PA layer is the reason for the surface roughness reduction [24]. It should be noted that reducing the surface roughness can improve the membrane fouling resistance. Upon increasing the concentration of zeolite introduced into the upper active layer and given the tendency of particles to clump together, we can expect a growth in the surface roughness. The RMS values in TFN-Z-0.01 and TFN-Z-0.02 membranes are 28.58 nm and 38.01 nm, respectively. Such an increase in the surface roughness has also been previously reported by other researchers [36].

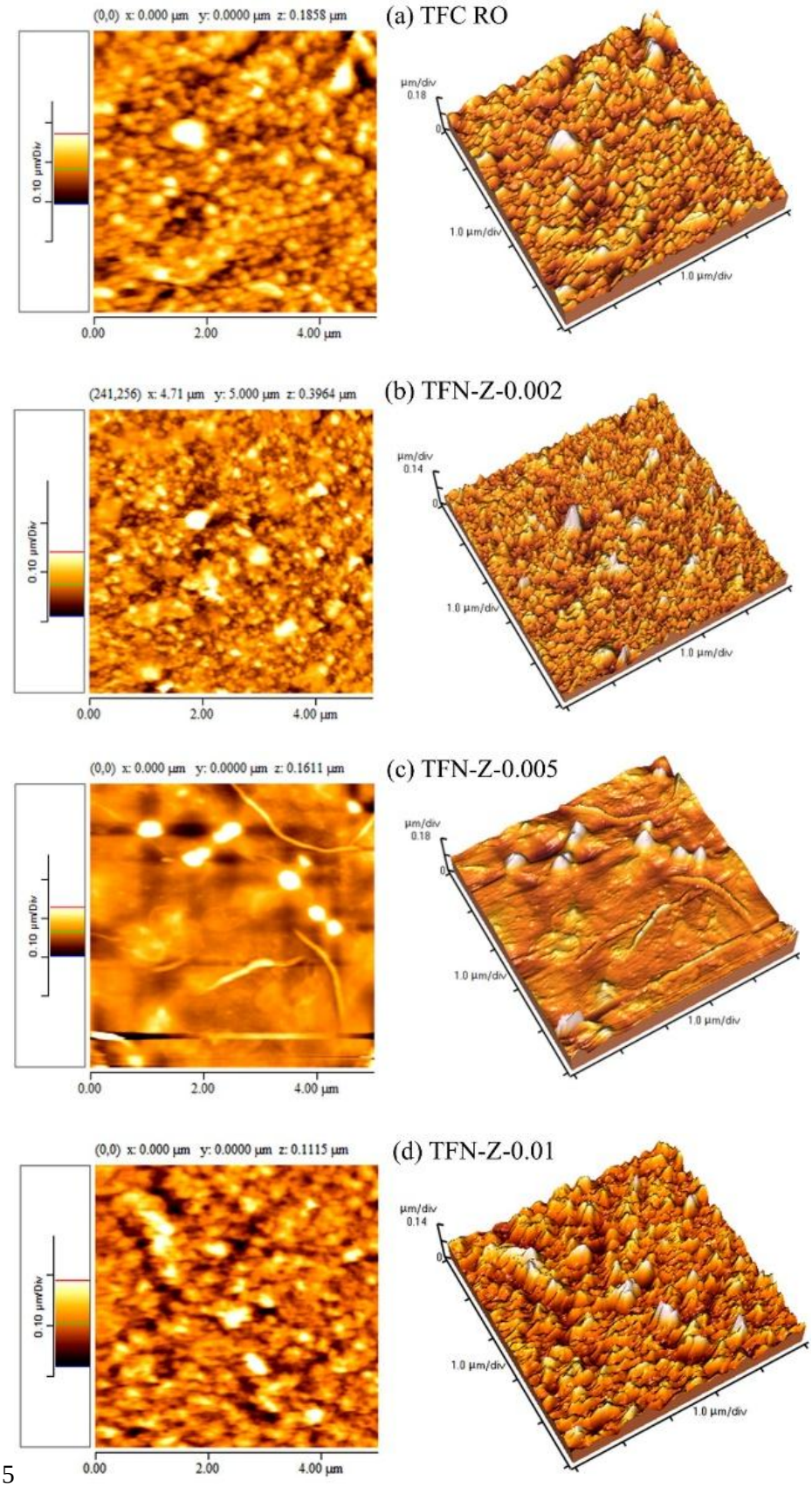
(0,0) x: 0.000 µm y: 0.0000 µm z: 0.1858 µm
(a) TFC RO
0.10 µm/Div
0.00
2.00
4.00 µm
µm/div
0.18
0
1.0 µm/div
1.0 µm/div
(241,256) x: 4.71 µm y: 5.000 µm z: 0.3964 µm
(b) TFN-Z-0.002
0.10 µm/Div
0.00
2.00
4.00 µm
µm/div
0.14
0
1.0 µm/div
1.0 µm/div
(0,0) x: 0.000 µm y: 0.0000 µm z: 0.1611 µm
(c) TFN-Z-0.005
0.10 µm/Div
0.00
2.00
4.00 µm
µm/div
0.18
0
1.0 µm/div
1.0 µm/div
(0,0) x: 0.000 µm y: 0.0000 µm z: 0.1115 µm
(d) TFN-Z-0.01
0.10 µm/Div
0.00
2.00
4.00 µm
µm/div
0.14
0
1.0 µm/div
1.0 µm/div

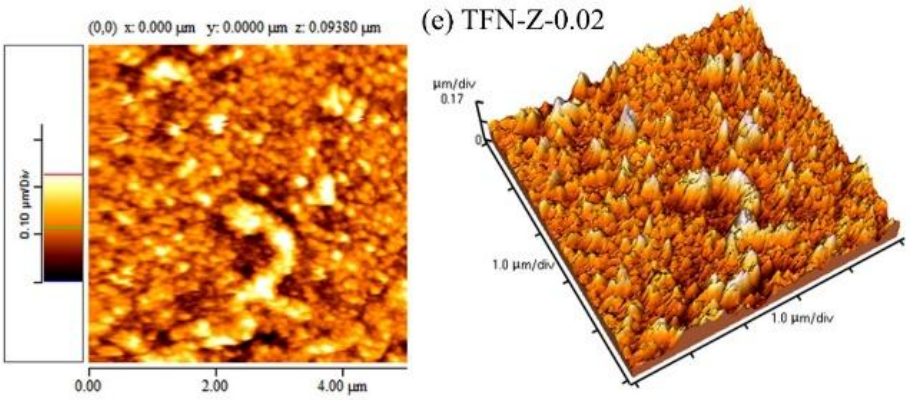

Figure 5. Two- and three-dimensional AFM images of (a) TFC, (b) TFN-Z-0.002, (c) TFN-Z-0.005, (d) TFN-Z-0.01, and (e) TFN-Z-0.02 membranes

Table 1. The surface roughness parameters of the fabricated membranes (5 µm × 5 µm)

Membrane	Roughness parameters	
	RMS (nm)	R_a (nm)
TFC	29.73	22.74
TFN-Z-0.002	21.81	16.15
TFN-Z-0.005	21.05	13.15
TFN-Z-0.01	28.58	21.98
TFN-Z-0.02	38.01	29.18

The surface functional groups of TFC and TFN-Z-0.005 membranes was investigated using the ATR-FTIR analysis. This test makes it possible to pursue the chemical bonds of the membranes. As observed in Figure 6, both membranes have similar absorption bands; however, the appearance of a weak band at 667 cm^{-1} in TFN-Z-0.005 membrane shows the presence of TiO_2. This band in the FTIR analysis is observed at 628 cm^{-1}. This shift may be related to the probable interaction between the active layer and zeolite. Such shift has also been reported in other reseraches in the literature [60]. The characteristic bands at 1548 and 1606 cm^{-1} correspond to the vibration of the amide II and aromatic ring, respectively. These peaks show the formation of the PA layer on the PSf support [39]. The band at 3361 cm^{-1} belongs to the hydroxyl group, and the appearing bands in the range of 1078-1235 cm^{-1} are attributed to the C–N bendings. The bands at 831 and 1485 cm^{-1} appear due to the deformation vibrations of phenyl groups with 1,4 substitution and aromatic ring stretches, respectively. In addition, the bands at 852 and 872 cm^{-1} are attibuted to the characteristics of aromatic hydrogen. The strong band at 1583 cm^{-1} is formed due to the aromatic in-plane ring vibration. The band at 2964 cm^{-1} corresponds to the aromatic C–H stretching and in-plane bending and that at 1502 cm^{-1} to the stretching mode of C=C [61-63].

Figure 7 lists the contact angles of the fabricated membranes important parameters that play a key role in determining the membrane hydrophilicity. The smaller

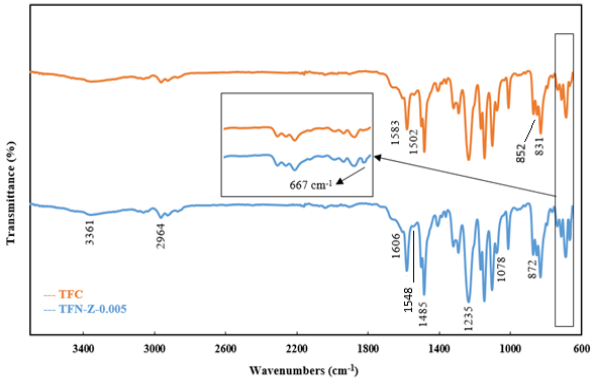

Figure 6. ATR-FTIR spectra of TFC and TFN-Z-0.005 membranes

the contact angle, the higher the hydrophilicity of the membrane. The TFC membrane has a contact angle of 64.44° that decrease with zeolite embedment. The contact angle of TFN-Z-0.005 is 51.32°. The high affinity of TiO_2 group with the negative charge for water molecules is the reason for such a decrease [64]. The contact angles increases upon increasing the zeolite content in both TFN-Z-0.01 and TFN-Z-0.02 membranes. Such behavior results from the aggregation of zeolite particles on the membrane surface under high loadings which in turn leads to a reduction in the effective contact surface of zeolite and consequently membrane hydrophilicity [65].

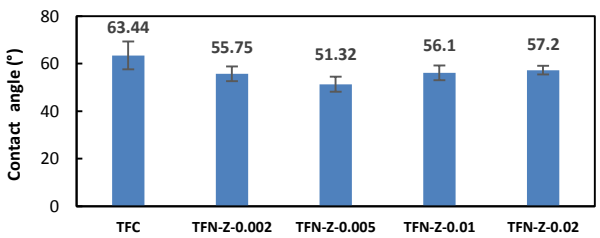

Figure 7. Water contact angle of the TFC membranes PI

3.3. Filtration Performance

In order to evaluate the performance of the fabricated membranes with different zeolite concentrations, the pure water flux values as well as the desalination performance were investigated. Figure 8 presents the water flux of all membranes as a function of the zeolite concentration embedded in the polymer matrix.

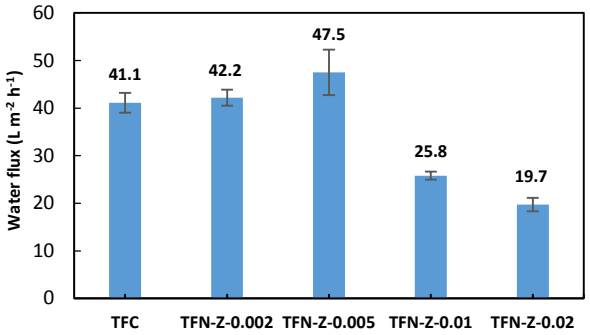

Figure 8. Effect of zeolite concentration on water flux of the fabricated TFC membranes

As reflected, the water flux value for the TFC membrane was obtained as 41.1 $Lm^{-2}h^{-1}$, which grew up to 47.5 $Lm^{-2}h^{-1}$ at the optimal zeolite concentration of 0.005 wt. %. Upon increasing the concentration of the incorporated zeolite, the water flux would sharply decrease. According to Figure 8, the water flux of TFN-Z-0.01 and TFN-Z-0.02 membranes equal 25.8 and 19.7 $Lm^{-2}h^{-1}$, respectively. Improvements in the performance of composite membranes containing nanomaterials were made as a result of variations in the morphology or membrane surface roughness, changes in the PA film cross-linking degree, creation of the preferential diffusion paths for water molecules passage, and changes in the hydrophilicity of the membrane surface with the entry of particles with desirable functional groups such as hydroxyl [66]. In this study, TS-1 zeolite with a three-dimensional pore network larger than water molecules allowed more water to pass through the zeolite-containing membranes compared to the TFC membrane. It should be noted that the presence of extraframework titanium with hydroxyl groups and high affinity to water molecules is another factor that can decrease the water flux. In other words, the bonding between hydroxyl groups of TiO_2 and hydrogen groups in water molecules would improve the membrane hydrophilicity. However, an increase in the zeolite content has a negative effect on water diffusion. With agglomeration and improper distribution of zeolite particles at high concentrations, the amount of effective available pores for the transport of water molecules is reduced, hence a decrease in the water flux [67,68].

To better evaluate the performance of zeolite, the results of salt rejection should be taken into consideration. Figure 9 presents the NaCl rejection values. While the rejection amount in the TFC membrane was 95.01 %, it increased up to 96.78 % with the embedment of 0.005 wt. % zeolite. Negative surface charges of the membranes containing zeolite resulting from the presence of hydroxyl groups of TiO_2 on TS-1 made the electrostatic repulsion reject NaCl. Of note, the pore size of zeolite is smaller than those of Na^+ and Cl^- ions which leads to higher rejection in the TFN membranes than in the TFC. To be specific, the pore size of TS-1 zeolite is 5.6 nm × 5.3 nm [42], and the diameters of the hydrated sodium and chlorine ions are 0.716 nm and 0.664 nm, respectively [69]. The presence of such a pore size will restrict the transport of salt ions. Contrarily, at high concentrations of zeolite, blockage of membranes pores caused by agglomeration of zeolite particles led to an increase in the resistance of TFN-Z-0.01 and TFN-Z-0.02 membranes to the salt passage.

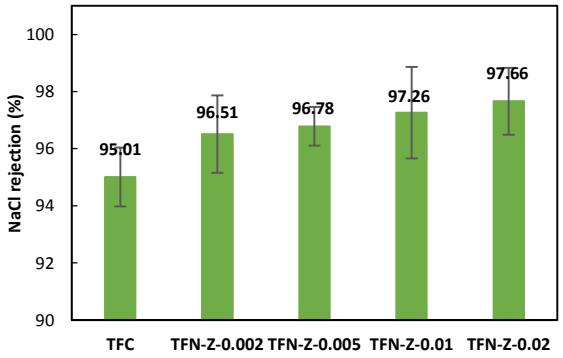

Figure 9. NaCl salt rejection of the fabricated TFC membranes

3.4. Antifouling Performance

Figure 10 shows the antifouling ability of all membranes. The results obtained from examining the a saline solution of 2000 ppm NaCl and 200 ppm BSA indicated that the TFC membrane had the highest flux reduction in the 90 min filtration test, compared to the initial flux. The flux drop in this membrane was 21 % in relation to the initial flux value. However, once TS-1 zeolite was added to the thin active layer, the layer showed high resistance to fouling. In other words, in all membranes containing zeolite, a decrease of less than 10 % of the final flux was observed compared to the flux in the first 10 min filtration. Given that the accumulation of foulants on the membrane surface weakens its performance and increases the operating costs, antifouling potential in the RO membranes gains more significance than ever. Some factors such as feed water properties, hydrodynamic conditions, and membrane surface properties cause fouling [5,10]. Foulant adsorption occurs as a result of the interactions between the membrane surface and foulant as well as some membrane properties such as affinity to water, surface charge, and topology. Increased membrane

hydrophilicity due to the nature of many precipitators can improve membrane fouling resistance.

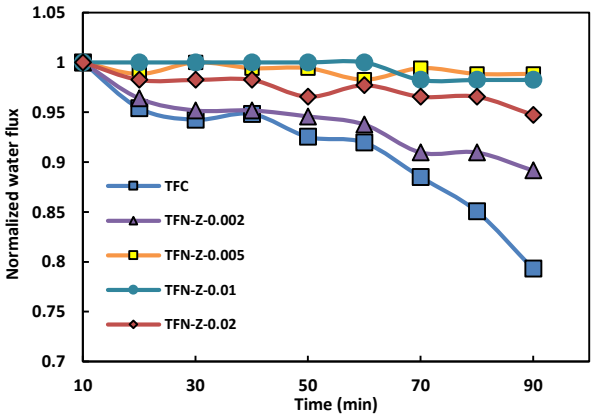

Figure 10. Normalized water flux as a function of BSA/NaCl solution filtration time

Hydrophilic membranes with high surface tensions are able to form hydrogen bonds with the surrounding water molecules which can create an aqueous boundary between the membrane and bulk solution, thus making a severe restriction for the hydrophobic solvent approaching the membrane surface. In case the foulant charge and membrane surface are similar, the electrostatic repulsion force between the membrane and foulant prevents fouling. Increasing the surface negative charge by incorporating functionalities such as hydroxyl can increase the repulsive force with negatively charged foulants namely protein that will subsequentially reduce the membrane fouling. Another important factor in fouling is the roughness of the membrane surfaces. Increased roughness may lead to the formation of a boundary layer or uneven flow distribution on the surface and expand the surface area, thus facilitating the accumulation of foulants on the surface [5]. In membranes containing TS-1 zeolite, the presence of TiO_2 in the PA layer prevents the protein from approaching and adhering to the surface of the membrane by creating a strong repulsive force caused by negative charges to the BSA and also increasing hydrophilicity. In the TFN-Z-0.005 membrane which has the lowest surface roughness according to AFM analysis, the least flux reduction as a result of fouling is observed, indicating an excellent resistance to fouling. In contrast, TFN-Z-0.01 and TFN-Z-0.02 membranes with quite high roughness due to agglomeration of zeolite particles show high resistance to fouling, which may be attributed to the high negative charge density and excretion.

4. CONCLUSION

In this study, TS-1 zeolite with the mean particle size of 180 nm was synthesized based on the hydrothermal method and then added to the polymerization solution to be inserted into a thin film layer of RO composite membranes. The EDX analysis confirmed the presence and relatively uniform distribution of zeolite in the PA layer. The results from the ATR-FTIR analysis also confirmed the presence of TiO_2 on the membrane. Characterized by the hydrophilicity and pore size larger than that of the water molecules at 0.005 wt. % as the optimal concentration of zeolite, the water flux rised from 41.1 $Lm^{-2}h^{-1}$ up to 47.5 $Lm^{-2}h^{-1}$ in the TFC membrane. Evaluation of the findings of the filtration experiments in the membranes containing zeolite indicated their enhanced separation performance and high antifouling potential owing to the negative surface charge produced by TiO_2.

ACKNOWLEDGEMENTS

The authors are grateful to both Arak and Kharazmi Universities for the all supports throughout this research.

NOMENCLATURE

AFM	Atomic Force Microscopy
ATR-FTIR	Attenuated Total Reflection-Fourier Transform Infrared
BSA	Bovine Serum Albumin
CNTs	Carbon Nanotubes
CSA	(+) 10-camphor sulfonic acid
DMF	Dimethylformamide
EDX	Energy Dispersive X-ray
FE-SEM	Field Emission Scanning Electron Microscopy
FTIR	Fourier Transform Infrared spectroscopy
GO	Graphene Oxide
IP	Interfacial Polymerization
MOFs	Metal-Organic Frameworks
MPD	M-Phenylene Diamine
PA	Polyamide
PSf	Polysulfone
RMS	Root Mean Square roughness
RO	Reverse Osmosis
S_a	Average arithmetic roughness
TBOT	Tetra-n-Butyl Orthotitanate
TEA	Triethylamine
TEOS	Tetraethyl orthosilicate
TFC	Thin Film Composite membranes
TFN	Thin Film Nanocomposite
TiO_2	Titanium dioxide
TMC	Tri-Mesoyl Chloride
TPAOH	Tetrapropylammonium hydroxide
TS-1	Titanium silicate-1
XRD	X-Ray Diffraction

REFERENCES

1. Shenvi, S. S., Isloor, A. M., Ismail, A. F., "A review on RO membrane technology: Developments and challenges", ***Desalination***, Vol. 368, (2015), 10-26. https://doi.org/10.1016/j.desal.2014.12.042
2. Hailemariam, R. H., Woo, Y. C., Damtie, M. M., Kim, B. C., Park,

K. D., Choi, J. S., "Reverse osmosis membrane fabrication and modification technologies and future trends: A review", ***Advances in Colloid and Interface Science***, Vol. 276, (2020), 102100. https://doi.org/10.1016/j.cis.2019.102100

3. Greenlee, L. F., Lawler, D. F., Freeman, B. D., Marrot, B, Moulin, P., "Reverse osmosis desalination: Water sources, technology, and today's challenges", ***Water Research***, Vol. 43, No. 9, (2009), 2317-2348. https://doi.org/10.1016/j.watres.2009.03.010
4. Elimelech, M., Phillip, W. A., "The future of seawater desalination: Energy, technology, and the environment", ***Science***, Vol. 333, No. 6043, (2011), 712-717. https://doi.org/10.1126/science.1200488
5. Asadollahi, M., Bastani, D., Musavi, S. A., "Enhancement of surface properties and performance of reverse osmosis membranes after surface modification: A review", ***Desalination***, Vol. 420, (2017), 330-383. https://doi.org/10.1016/j.desal.2017.05.027
6. Cay-Durgun, P., Lind, M. L., "Nanoporous materials in polymeric membranes for desalination", ***Current Opinion in Chemical Engineering***, Vol. 20, (2018), 19-27. https://doi.org/10.1016/j.coche.2018.01.001
7. Al-Karaghouli, A. A., Kazmerski, L. L., "Renewable energy opportunities in water desalination", In Schorr, M. (ed.), ***Desalination, Trends and Technologies***, London, IntechOpen, (2011), 149-184. https://doi.org/10.5772/14779
8. Lee, K. P., Arnot, T. C., Mattia, D., "A review of reverse osmosis membrane materials for desalination—development to date and future potential", ***Journal of Membrane Science***, Vol. 370, No. 1-2, (2011), 1-22. https://doi.org/10.1016/j.memsci.2010.12.036
9. Wang, Y. N., Wang, R., "Reverse osmosis membrane separation technology, In ***Membrane Separation Principles and Applications***, (2019), 1-45. https://doi.org/10.1016/B978-0-12-812815-2.00001-6
10. Jiang, S., Li, Y., Ladewig, B. P., "A review of reverse osmosis membrane fouling and control strategies", ***Science of the Total Environment***, Vol. 595, (2017), 567-583. https://doi.org/10.1016/j.scitotenv.2017.03.235
11. Jhaveri, J. H., Murthy, Z. V. P., "A comprehensive review on anti-fouling nanocomposite membranes for pressure driven membrane separation processes", ***Desalination***, Vol. 379, (2016), 137-154. https://doi.org/10.1016/j.desal.2015.11.009
12. Park, S. J., Kwon, S. J., Kwon, H. E., Shin, M. G., Park, S. H., Park, H., Park, Y. I., Nam, S. E., Lee, J. H., "Aromatic solvent-assisted interfacial polymerization to prepare high performance thin film composite reverse osmosis membranes based on hydrophilic supports", ***Polymer***, Vol. 144, (2018), 159-167. https://doi.org/10.1016/j.polymer.2018.04.060
13. Zhang, Z., Qin, Y., Kang, G., Yu, H., Jin, Y., Cao, Y., "Tailoring the internal void structure of polyamide films to achieve highly permeable reverse osmosis membranes for water desalination", ***Journal of Membrane Science***, Vol. 595, (2020), 117518. https://doi.org/10.1016/j.memsci.2019.117518
14. Zhang, Y., Wan, Y., Pan, G., Shi, H., Yan, H., Xu, J., Guo, M., Wang, Z., Liu, Y., "Surface modification of polyamide reverse osmosis membrane with sulfonated polyvinyl alcohol for antifouling", ***Applied Surface Science***, Vol. 419, (2017), 177-187. https://doi.org/10.1016/j.apsusc.2017.05.047
15. Reis, R., Duke, M., Merenda, A., Winther-Jensen, B., Puskar, L., Tobin, M. J., Orbell, J. D., Dumée, L. F., "Customizing the surface charge of thin-film composite membranes by surface plasma thin film polymerization", ***Journal of Membrane Science***, Vol. 537, (2017), 1-10. https://doi.org/10.1016/j.memsci.2017.05.013
16. Vatanpour, V., Zoqi, N., "Surface modification of commercial seawater reverse osmosis membranes by grafting of hydrophilic monomer blended with carboxylated multiwalled carbon nanotubes", ***Applied Surface Science***, Vol. 396, (2017), 1478-1489. https://doi.org/10.1016/j.apsusc.2016.11.195
17. Saleem, H., Zaidi, S. J., "Nanoparticles in reverse osmosis membranes for desalination: A state of the art review", ***Desalination***, Vol. 475, (2020), 114171. https://doi.org/10.1016/j.desal.2019.114171
18. Mallya, D. S., Yang, G., Lei, W., Muthukumaran, S., Baskaran, K., "Functionalized mos2 nanosheets enabled nanofiltration membrane with enhanced permeance and fouling resistance", ***Environmental Technology & Innovation***, Vol. 27, (2022), 102719. https://doi.org/10.1016/j.eti.2022.102719
19. Tong, Y., Wang, Y., Bian, S., Ge, H., Xiao, F., Li, L., Gao, C., Zhu, G., "Incorporating ag@ RF core-shell nanomaterials into the thin film nanocomposite membrane to improve permeability and long-term antibacterial properties for nanofiltration", ***Science of The Total Environment***, Vol. 839, (2022), 156231. https://doi.org/10.1016/j.scitotenv.2022.156231
20. Wu, C., Xie, Q., Hong, Z., Shen, L., Yu, T., Guo, H., Xiong, Y., Zhang, G., Lu, Y., Shao, W., "Thin-film nanocomposite nanofiltration membrane with enhanced desalination and antifouling performance via incorporating l-aspartic acid functionalized graphene quantum dots", ***Desalination***, Vol. 498, (2021), 114811. https://doi.org/10.1016/j.desal.2020.114811
21. Liao, Z., Zhu, J., Li, X., Van der Bruggen, B., "Regulating composition and structure of nanofillers in thin film nanocomposite (TFN) membranes for enhanced separation performance: A critical review", ***Separation and Purification Technology***, Vol. 266, (2021), 118567. https://doi.org/10.1016/j.seppur.2021.118567
22. Wang, Y., Meng, X., Wu, H., Bian, S., Tong, Y., Gao, C., Zhu, G., "Improving permeability and anti-fouling performance in reverse osmosis application of polyamide thin film nanocomposite membrane modified with functionalized carbon nanospheres", ***Separation and Purification Technology***, Vol. 270, (2021), 118828. https://doi.org/10.1016/j.seppur.2021.118828
23. El-Aassar, A. H. M. A., "Improvement of reverse osmosis performance of polyamide thin-film composite membranes using tio_2 nanoparticles", ***Desalination and Water Treatment***, Vol. 55, No. 11, (2015), 2939-2950. https://doi.org/10.1080/19443994.2014.940206
24. Safarpour, M., Khataee, A., Vatanpour, V., "Thin film nanocomposite reverse osmosis membrane modified by reduced graphene oxide/tio2 with improved desalination performance", ***Journal of Membrane Science***, Vol. 489, (2015), 43-54. https://doi.org/10.1016/j.memsci.2015.04.010
25. Al Mayyahi, A., "TiO_2 polyamide thin film nanocomposite reverses osmosis membrane for water desalination", ***Membranes***, Vol. 8, No. 3, (2018), 66. https://doi.org/10.3390/membranes8030066
26. Chae, H. R., Lee, J., Lee, C. H., Kim, I. C., Park, P. K., "Graphene oxide-embedded thin-film composite reverse osmosis membrane with high flux, anti-biofouling, and chlorine resistance", ***Journal of Membrane Science***, Vol. 483, (2015), 128-135. https://doi.org/10.1016/j.memsci.2015.02.045
27. Baek, Y., Kim, H. J., Kim, S. H., Lee, J. C., Yoon, J., "Evaluation of carbon nanotube-polyamide thin-film nanocomposite reverse osmosis membrane: Surface properties, performance characteristics and fouling behavior", ***Journal of Industrial and Engineering Chemistry***, Vol. 56, (2017), 327-334. https://doi.org/10.1016/j.jiec.2017.07.028
28. Liu, Y., Wang, X. P., Zong, Z. A., Lin, R., Zhang, X. Y., Chen, F. S., Zhang, L. L., Meng, X. M., Hou, J., "Thin film nanocomposite membrane incorporated with 2D-MOF nanosheets for highly efficient reverse osmosis desalination", ***Journal of Membrane Science***, Vol. 653, (2022), 120520. https://doi.org/10.1016/j.memsci.2022.120520
29. Shukla, A. K., Alam, J., Alhoshan, M. S., Ali, F. A. A., Mishra, U., Hamid, A. A., "Thin-film nanocomposite membrane incorporated with porous zn-based metal–organic frameworks: Toward enhancement of desalination performance and chlorine

resistance", ***ACS Applied Materials & Interfaces***, Vol. 13, No. 24, (2021), 28818-28831. https://doi.org/10.1021/acsami.1c05469

30. Safarpour, M., Vatanpour, V., Khataee, A., Zarrabi, H., Gholami, P., Yekavalangi, M. E., "High flux and fouling resistant reverse osmosis membrane modified with plasma treated natural zeolite", ***Desalination***, Vol. 411, (2017), 89-100. https://doi.org/10.1016/j.desal.2017.02.012
31. Dehghanpour, S. B., Parvizian, F., Vatanpour, V., He, T., "Enhancing the flux and salt rejection of thin-film composite nanofiltration membranes prepared on plasma-treated polyethylene using PVA/TS-1 composite", ***Reactive and Functional Polymers***, Vol. 177, (2022), 105329. https://doi.org/10.1016/j.reactfunctpolym.2022.105329
32. Bandehali, S., Parvizian, F., Moghadassi, A., Hosseini, S. M., "Chapter 5 - Nanomaterials for the efficient abatement of wastewater contaminants by means of reverse osmosis and nanofiltration, in Nanomaterials for the detection and removal of wastewater pollutants", In ***Nanomaterials for the Detection and Removal of Wastewater Pollutants***, Elsevier, (2020), 111-144. https://doi.org/10.1016/B978-0-12-818489-9.00005-0
33. Jeong, B. H., Hoek, E. M., Yan, Y., Subramani, A., Huang, X., Hurwitz, G., Ghosh, A. K, Jawor, A., "Interfacial polymerization of thin film nanocomposites: A new concept for reverse osmosis membranes", ***Journal of Membrane Science***, Vol. 294, No. 1-2, (2007), 1-7. https://doi.org/10.1016/j.memsci.2007.02.025
34. Fathizadeh, M., Aroujalian, A., Raisi, A., "Effect of added NaX nano-zeolite into polyamide as a top thin layer of membrane on water flux and salt rejection in a reverse osmosis process", ***Journal of Membrane Science***, Vol. 375, No. 1-2, (2011), 88-95. https://doi.org/10.1016/j.memsci.2011.03.017
35. Dong, H., Zhao, L., Zhang, L., Chen, H., Gao, C., Ho, W. W., "High-flux reverse osmosis membranes incorporated with NaY zeolite nanoparticles for brackish water desalination", ***Journal of Membrane Science***, Vol. 476, (2015), 373-383. https://doi.org/10.1016/j.memsci.2014.11.054
36. Cay-Durgun, P., McCloskey, C., Konecny, J., Khosravi, A., Lind, M. L., "Evaluation of thin film nanocomposite reverse osmosis membranes for long-term brackish water desalination performance", ***Desalination***, Vol. 404, (2017), 304-312. https://doi.org/10.1016/j.desal.2016.10.014
37. Marioryad, H., Ghaedi, A. M., Emadzadeh, D., Baneshi, M. M., Vafaei, A., Lau, W. J., "A thin film nanocomposite reverse osmosis membrane incorporated with S-Beta zeolite nanoparticles for water desalination", ***ChemistrySelect***, Vol. 5, No. 6, (2020), 1972-1975. https://doi.org/10.1002/slct.201904084
38. Liu, Y., Chen, X., "High permeability and salt rejection reverse osmosis by a zeolite nano-membrane", ***Physical Chemistry Chemical Physics***, Vol. 15, No. 18, (2013), 6817-6824. https://doi.org/10.1039/C3CP43854F
39. Li, D., He, L., Dong, D., Forsyth, M., Wang, H., "Preparation of silicalite–polyamide composite membranes for desalination", ***Asia-Pacific Journal of Chemical Engineering***, Vol. 7, No. 3, (2012), 434-441. https://doi.org/10.1002/apj.588
40. Huang, H., Qu, X., Ji, X., Gao, X., Zhang, L., Chen, H, Hou, L., "Acid and multivalent ion resistance of thin film nanocomposite ro membranes loaded with silicalite-1 nanozeolites", ***Journal of Materials Chemistry A***, Vol. 1, No. 37, (2013), 11343-11349. https://doi.org/10.1039/C3TA12199B
41. Taramasso, M., Perego, G., Notari, B., SnamProgetti S. p. A., ***Preparation of Porous Crystalline Synthetic Material Comprised of Silicon and Titanium Oxides***, U.S. Patent 4,410,501A, (1983). Available at: https://patents.google.com/patent/US4410501A/en (Accessed: 07 September 2022).
42. Clerici, M. G., "Titanium silicalite-1", In Jackson, D., Hargreaves, S. J., (eds.), ***Metal Oxide Catalysis***, (2008), 705-754. https://doi.org/10.1002/9783527626113.ch18
43. Zuo, Y., Song, W., Dai, C., He, Y., Wang, M., Wang, X., Guo, X., "Modification of small-crystal titanium silicalite-1 with organic bases: Recrystallization and catalytic properties in the hydroxylation of phenol", ***Applied Catalysis A: General***, Vol. 453, (2013), 272-279. https://doi.org/10.1016/j.apcata.2012.12.027
44. Chen, L., Wang, Y. M., He, M. Y., "Hydrothermal synthesis of hierarchical titanium silicalite-1 using single template", ***Materials Research Bulletin***, Vol. 46, No. 5, (2011), 698-701. https://doi.org/10.1016/j.materresbull.2011.01.015
45. Han, X., Zhang, X., Ma, X., Li, J., "TS-1 molecular sieves filled polydimethylsiloxane membranes for ethanol/water separation via pervaporation", ***Polymer Engineering & Science***, Vol. 56, No. 5, (2016), 583-589. https://doi.org/10.1002/pen.24283
46. Martin-Gil, V., Lopez, A., Hrabanek, P., Mallada, R., Vankelecom, I. F. J., Fila, V., "Study of different titanosilicate (TS-1 and ETS-10) as fillers for mixed matrix membranes for CO_2/CH_4 gas separation applications", ***Journal of Membrane Science***, Vol. 523, (2017), 24-35. https://doi.org/10.1016/j.memsci.2016.09.041
47. Zhang, Q., Liu, Y., Liu, X., Ma, L., "Facile preparation of bilayer titanium silicate (TS-1) zeolite membranes by periodical secondary growth", ***Coatings***, Vol. 9, No. 12, (2019), 850. https://doi.org/10.3390/coatings9120850
48. Du, Q., Guo, Y., Duan, H., Li, H., Chen, Y., Liu, H., "Synthesis of hierarchical ts-1 zeolite via a novel three-step crystallization method and its excellent catalytic performance in oxidative desulfurization", ***Fuel***, Vol. 188, (2017), 232-238. https://doi.org/10.1016/j.fuel.2016.10.045
49. Zuo, Y., Liu, M., Zhang, T., Meng, C., Guo, X., Song, C., "Enhanced catalytic performance of titanium silicalite-1 in tuning the crystal size in the range 1200–200 nm in a tetrapropylammonium bromide system", ***ChemCatChem***, Vol. 7, No. 17, (2015), 2660-2668. https://doi.org/10.1002/cctc.201500440
50. Liu, M., Chang, Z., Wei, H., Li, B., Wang, X., Wen, Y., "Low-cost synthesis of size-controlled ts-1 by using suspended seeds: From screening to scale-up", ***Applied Catalysis A: General***, Vol. 525, (2016), 59-67. https://doi.org/10.1016/j.apcata.2016.07.006
51. Du, Q., Guo, Y., Wu, P., Liu, H., Chen, Y., "Facile synthesis of hierarchical TS-1 zeolite without using mesopore templates and its application in deep oxidative desulfurization", ***Microporous and Mesoporous Materials***, Vol. 275, (2019), 61-68. https://doi.org/10.1016/j.micromeso.2018.08.018
52. Astorino, E., Peri, J. B., Willey, R. J., Busca, G., "Spectroscopic characterization of silicalite-1 and titanium silicalite-1", ***Journal of Catalysis***, Vol. 157, No. 2, (1995), 482-500. https://doi.org/10.1006/jcat.1995.1313
53. Tekin, D., Birhan, D., Kiziltas, H., "Thermal, photocatalytic, and antibacterial properties of calcinated nano-TiO_2/polymer composites", ***Materials Chemistry and Physics***, Vol. 251, (2020), 123067. https://doi.org/10.1016/j.matchemphys.2020.123067
54. Bandehali, S., Moghadassi, A., Parvizian, F., Shen, J., Hosseini, S. M., "Glycidyl POSS-functionalized ZnO nanoparticles incorporated polyether-imide based nanofiltration membranes for heavy metal ions removal from water", ***Korean Journal of Chemical Engineering***, Vol. 37, No. 2, (2020), 263-273. https://doi.org/10.1007/s11814-019-0441-5
55. Xue, T., Liu, H., Wang, Y., Wu, H., Wu, P., He, M., "Seed-induced synthesis of small-crystal TS-1 using ammonia as alkali source", ***Chinese Journal of Catalysis***, Vol. 36, No. 11, (2015), 1928-1935. https://doi.org/10.1016/S1872-2067(15)60955-X
56. Lin, J., Yang, T., Lin, C., Sun, J., "Hierarchical MFI zeolite synthesized via regulating the kinetic of dissolution-recrystallization and their catalytic properties", ***Catalysis Communications***, Vol. 115, (2018), 82-86. https://doi.org/10.1016/j.catcom.2018.07.006
57. Notari, B., "Microporous crystalline titanium silicates", In

Advances in Catalysis, Academic Press, Vol. 41, (1996), 253-334. https://doi.org/10.1016/S0360-0564(08)60042-5

58. Namvar-Mahboub, M., Pakizeh, M., Davari, S., "Preparation and characterization of UZM-5/polyamide thin film nanocomposite membrane for dewaxing solvent recovery", ***Journal of Membrane Science***, Vol. 459, (2014), 22-32. https://doi.org/10.1016/j.memsci.2014.02.014
59. Wang, L., Fang, M., Liu, J., He, J., Deng, L., Li, J., Lei, J., "The influence of dispersed phases on polyamide/ZIF-8 nanofiltration membranes for dye removal from water", ***RSC Advances***, Vol. 5, No. 63, (2015), 50942-50954. https://doi.org/10.1039/C5RA06185G
60. Vatanpour, V., Madaeni, S. S., Khataee, A. R., Salehi, E., Zinadini, S., Monfared, H. A., "TiO_2 embedded mixed matrix PES nanocomposite membranes: Influence of different sizes and types of nanoparticles on antifouling and performance", ***Desalination***, Vol. 292, (2012), 19-29. https://doi.org/10.1016/j.desal.2012.02.006
61. Huang, H., Qu, X., Dong, H., Zhang, L., Chen, H., "Role of NaA zeolites in the interfacial polymerization process towards a polyamide nanocomposite reverse osmosis membrane", ***RSC Advances***, Vol. 3, No. 22, (2013), 8203-8207. https://doi.org/10.1039/C3RA40960K
62. Abdel-Hameed, M., ElFadl, M. M. A., Ali, M. E., Kotp, Y. H., Shawky, H. A., "Effect of manufacture conditions on reverse osmosis desalination performance of polyamide thin film composite membrane and their spiral wound element", ***Desalination and Water Treatment***, Vol. 69, (2017), 65-71. https://doi.org/10.5004/dwt.2017.20293
63. Gryta, M., Bastrzyk, J., Lech, D., "Evaluation of fouling potential of nanofiltration membranes based on the dynamic contact angle measurements", ***Polish Journal of Chemical Technology***, Vol. 14, No. 3, (2012), 97-104. https://doi.org/10.2478/v10026-012-0091-4
64. Safarpour, M., Vatanpour, V., Khataee, A., "Preparation and characterization of graphene oxide/TiO_2 blended PES nanofiltration membrane with improved antifouling and separation performance", ***Desalination***, Vol. 393, (2016), 65-78. https://doi.org/10.1016/j.desal.2015.07.003
65. Anis, S. F., Hashaikeh, R., Hilal, N., "Flux and salt rejection enhancement of polyvinyl (alcohol) reverse osmosis membranes using nano-zeolite", ***Desalination***, Vol. 470, (2019), 114104. https://doi.org/10.1016/j.desal.2019.114104
66. Wang, F., Zheng, T., Xiong, R., Wang, P., Ma, J., "Strong improvement of reverse osmosis polyamide membrane performance by addition of ZIF-8 nanoparticles: Effect of particle size and dispersion in selective layer", ***Chemosphere***, Vol. 233, (2019), 524-531. https://doi.org/10.1016/j.chemosphere.2019.06.008
67. Borjigin, B., Yu, L., Xu, L., Zhao, C., Wang, J., "Influence of incorporating beta zeolite nanoparticles on water permeability and ion selectivity of polyamide nanofiltration membranes", ***Journal of Environmental Sciences***, Vol. 98, (2020), 77-84. https://doi.org/10.1016/j.jes.2020.04.010
68. Parvizian, F., Ansari, F., Bandehali, S., "Oleic acid-functionalized TiO_2 nanoparticles for fabrication of PES-based nanofiltration membranes", ***Chemical Engineering Research and Design***, Vol. 156, (2020), 433-441. https://doi.org/10.1016/j.cherd.2020.02.019
69. Duke, M. C., Zhu, B., Doherty, C. M., Hill, M. R., Hill, A. J., Carreon, M. A., "Structural effects on SAPO-34 and ZIF-8 materials exposed to seawater solutions, and their potential as desalination membranes", ***Desalination***, Vol. 377, (2016), 128-137. https://doi.org/10.1016/j.desal.2015.09.004